Automated GPS Signal-in-Space Anomalies Monitoring Over More than 11 Years

J. Sanz[1], J. M. Juan[1], C. López de Echazarreta[2], G. Gonzalez-Casado[1], A. Rovira García[1], M.T. Alonso[1], Deimos Ibáñez[1]
[1]*Research Group of Astronomy and Geomatics (gAGE/UPC)*
[2]*European Space Agency (ESA)*

BIOGRAPHIES

Dr. J. Sanz Subirana is senior researcher at gAGE/UPC. His current research interests are in the area of GNSS data processing algorithms, GNSS ionospheric sounding, augmentation systems (SBAS and GBAS), and High Accuracy GNSS Navigation.
Dr. J.M. Juan Zornoza is senior researcher at gAGE/UPC. His current research interests are in the area of GNSS data processing Algorithms for High Accuracy GNSS Navigation and GNSS ionospheric sounding, as well as Augmentation Systems.
C. López de Echazarreta is currently the EGNOS System Performance Principal Engineer at ESA. He holds a M.Sc. in Telecommunication Engineering and a Master in Space Technology both by the Polytechnic University of Madrid (Spain).
Dr. G. González Casado is senior researcher at gAGE/UPC. His current research interests are GNSS data processing and ionospheric sounding, high accuracy GNSS Navigation and Augmentation Systems (SBAS and GBAS).
Dr. A. Rovira García is a Marie Sklodowska-Curie fellow at gAGE/UPC. He co-authors 9 papers in peer-reviewed journals, 2 book chapters and over 20 works in meeting proceedings, with 1 best presentation award from the US Institute of Navigation.
Maria Teresa Alonso is a research mathematician in gAGE/UPC. She holds MS degree in Astronomy and Geodesy, in the Faculty of mathematics at Complutense University of Madrid (Spain). She is giving support to the GNSS projects.
Deimos Ibáñez is a research engineer at gAGE/UPC. He is the main developer of the gLAB Tool Suite, involving GNSS high precision, SBAS and DGNSS navigation. His current research topics are multi-constellation and SBAS applications.

ABSTRACT

This paper presents the results of a performance assessment of GPS constellation based on the International GNSS Service (IGS) data collected from 2004 to 2014. There exist previous analysis of GPS Signal-in-Space (SiS) anomalies which performed the screen out by comparing the broadcast GPS ephemerides and clocks with the precise data provided by IGS or by the National Geospatial-Intelligence Agency (NGA). In this paper, a complementary detection methodology has been developed which targets to detect very short duration events linked to satellite clock and pseudorange jumps. These SiS events are assessed by examining code and carrier phase measurements for a minimum set of IGS receivers worldwide distributed. Short duration (few seconds) satellite clock events are monitored using carrier measurements corrected by the geometric range and linearly interpolated precise satellite clocks at 300 seconds sampling rate. Pseudorange jumps are monitored with the code-minus-carrier combination, where the geometry and frequency dependent effects are removed. Events detected simultaneously on several receivers are recorded, while events that are not confirmed are discarded as receiver artefacts.

The results obtained following the application of the methodology are shown in order to offer an overview of the different events and their magnitudes. A total of 124 days with short duration clock events have been detected during the 11 years period analyzed. These events involve 23 GPS satellites, being 72 of such days associated to SVN063. No multiple satellite events have been found in the same day. It is also shown that the implemented code monitor is strongly affected by code multipath and, among all detections, only one code pseudorange jump event has been found, affecting the P1 of satellite SVN 061.

INTRODUCTION

Global Positioning Service provides free positioning and timing services worldwide for hundreds of millions users. Since the declaration of the Initial Operating Capability (IOC) in December 1993 with 24 operational satellites in orbit, and the Full Operational Capability (FOC) in June 1995, Global Positioning System (GPS) reliability and performances have been improving gradually, exceeding the minimum performance levels specified in the GPS Standard Positioning Service (SPS) [1].

https://doi.org/10.33012/2018.15853

Several GNSS integrity monitoring systems such as the Aircraft Based Augmentation System (ABAS), the Ground Based Augmentation Systems (GBAS) or the Satellite Based Augmentation System (SBAS), make use of the broadcast GPS Signal In Space (SiS) to provide their service. In this context, having a good knowledge of the GPS SiS anomalies is of great importance, not only for assessing the GPS reliability itself, but also for validating external assumptions used in the design of the above mentioned integrity monitoring systems.

There exist previous analysis of GPS SiS anomalies that performed the screen out by comparing the broadcast GPS ephemerides and clocks with the precise data provided by the International GNSS Service (IGS) or the National Geospatial-Intelligence Agency (NGA) [2], [3]-[5].

In this paper, a complementary detection methodology is presented which is based on the use of code and carrier-phase measurements available from a set of IGS receivers worldwide distributed. The proposed methodology targets to detect very short duration events (with time scales of few seconds) which most of them are undetectable through the processing of the IGS products.

This paper provides the results of the assessment of IGS GPS data collected from 2004 to 2014 focusing on the following list of SiS anomalies: satellite clock and code-carrier incoherency events.

For each of the above mentioned SiS anomalies, an automated methodology of detection was developed and will be presented. The results obtained following the application of the methodology are shown in order to offer an overview of the different events and their magnitudes.

The present paper is organized as follows. First, it is presented the methodology implemented for each of the code and carrier-phase monitors. Then it summarizes the data-set used for the analysis, including selection of the receivers type, the orbit and clock products used for the analysis and their pre-processing. Next, it provides the results of the monitor's characterization, including the SiS events detected above a selected monitor threshold. Finally it is summarized the conclusions.

METHODOLOGY FOR THE SIGNAL IN SPACE EVENTS ANALYSIS

The definition of the Carrier-phase and Code monitors as well as the methodology for their identification and monitoring is given next.

Carrier-phase based monitor: Carrier Jump, Drift and Acceleration

Objective: To detect carrier jump, drift and acceleration events on individual frequencies and satellites. Identify anomalous behaviors.

This monitor (inspired in [6]) is mainly targeting to detect short duration events, i.e. with time scales of one or few seconds, that are undetectable with the IGS precise products, with sampling rates of 5 minutes. This monitor mainly accounts for the lack of linearity of satellite clocks within the clock update intervals (i.e. in between the five minutes clock samples).

Input data:

- RINEX observation files from GPS satellites covering the globe at 1Hz sampling rate, with 15º elevation mask.
- Precise satellite orbits and clocks from IGS at 15 minutes and 5 minutes, respectively. Orbits are interpolated by a 9-degree polynomial. Clocks are linearly interpolated.

Output data:

- Satellites with anomalous carrier jump, drift or acceleration values detected simultaneously by three or more receivers.
- Statistics for aggregated results for carrier jump, drift and acceleration errors.

Assumptions:

- Valid precise orbit and clock products are available.

Algorithm:

For each epoch (*t*)

For each receiver (*m*)

For each satellite (*n*)

- Compute corrected carrier phase by removing satellite clock and geometric range. We refer the computed value to the beginning of the observation arc value:

$$\Phi_{c,m,n}(t) = \Phi_{m,n}(t) - \rho_{m,n}(t) - \delta t_n\ (t) - \Phi_{ci,m,n}(0)$$
$$\Phi_{ci,m,n}(0) = \Phi_{m,n}(0) - \rho_{m,n}(0)\ - \delta t_n\ (0)$$

  where $\Phi_{m,n}$ is the measured carrier phase, $\rho_{m,n}$ is the geometric range (distance between satellite and receiver antenna phase centers), $\delta t_n\ (t)$ is the satellite clock and $\Phi_{ci,m,n}(0)$ is the carrier phase at the beginning of the observation arc.

  In case of cycle slip detection or in case of unavailable data (data gaps), the term $\Phi_{ci,m,n}(0)$ is reinitialized.

- Remove the receiver clock by computing Single Differences (SD) of corrected carriers with a reference satellite:

  Two different reference satellites are used to compute the SD, in order to discriminate if the anomalous behavior is linked to the satellite under testing or to the reference satellite and to identify the faulty satellite.

  The two highest elevation satellites, *R1* and *R2*, (excluding the satellite under testing) are taken as reference satellites.

$$\mathrm{D}\Phi^1_{\mathrm{c,m,n}}(\mathrm{t}) = \Phi_{\mathrm{c,m,n}}(\mathrm{t}) - \Phi_{\mathrm{c,m},R1}(\mathrm{t})$$
$$\mathrm{D}\Phi^2_{c,m,n}(t) = \Phi_{c,m,n}(t) - \Phi_{c,m,\mathrm{R2}}(t)$$

- Compute and record the carrier drift and acceleration by fitting a *second-degree polynomial* $p(t) = c_0 + c_1 t + c_2 t^2$ on 10 consecutive samples using the least squares method.

  The drift is given by the coefficient c_1 and acceleration by $2c_2$. Jump error is given by the difference between the real corrected carrier-phase determined for the next epoch and its predicted value with $p(t)$. Note: An independent fit is done for each SD: $\mathrm{D}\Phi^1_{c,m,n}(\mathrm{t})$ and $\mathrm{D}\Phi^2_{c,m,\mathrm{n}}(\mathrm{t})$, and for each L1, L2 carrier.

- Compute the MEDIAN and MINIMUM values for each epoch with three or more stations with the satellite in view. By default, they are computed with the polynomial fit of $\mathrm{D}\Phi^1_{c,m,n}(\mathrm{t})$, but when the values are over a predefined threshold, the polynomial fit of $\mathrm{D}\Phi^2_{c,m,n}(\mathrm{t})$ is used, whatever they are over the threshold or not.

- Anomalous behavior is declared at a given epoch *t* when the MEDIAN value of acceleration, ramp or jump is over a predefined threshold, for a given GPS carrier (L1 or L2).

Code based monitor: Code-Carrier Incoherency

Objective: To detect incoherency between code and carrier measurements, identified as steps over an interval of 100 seconds.

Input data:

- RINEX observation files from GPS satellites covering the globe at 1Hz sampling rate, with 20º elevation mask.

Output data:

- Satellites with anomalous code-minus-carrier values detected simultaneously by three or more receivers.
- Statistics for aggregated results for code-minus-carrier errors.

Assumptions:

- Carrier phase measurements are clean (no carrier events within the analysis period).
- As this monitor does not require orbit and clock products (i.e. geometry and clock are removed by a combination of carriers), the computations can be extended to a periods where precise orbits and clocks are not available. In any case, the quality of carriers and satellite's health are checked when analyzing the potential anomalies.

Algorithm:

For each epoch (*t*)

For each receiver (*m*)

For each satellite (*n*)

- Compute the following code-minus-carrier combination for each code:

GPS C1, P1 and P2 codes:

$$M_{P1_{m,n}}(t) = R_{P1_{m,n}}(t) - \Phi_{1_{m,n}}(t) - 2\frac{1}{\gamma_{12}-1}\left(\Phi_{1_{m,n}}(t) - \Phi_{2_{m,n}}(t)\right),$$

$$M_{P2_{m,n}}(t) = R_{P2_{m,n}}(t) - \Phi_{2_{m,n}}(t) - 2\frac{\gamma_{12}}{\gamma_{12}-1}\left(\Phi_{1_{m,n}}(t) - \Phi_{2_{m,n}}(t)\right),$$

where

$\Phi_{1_{m,n}}(t)$ is the measured carrier-phase on the L1 frequency,

$\Phi_{2_{m,n}}(t)$ is the measured carrier-phase on the L2 frequency,

$R_{P1_{m,n}}(t)$ is the measured P1 or C1 code on the first frequency,

$R_{P2_{m,n}}(t)$ is the measured P2 code on the second frequency

and $\gamma_{12} = \left(\frac{f_1}{f_2}\right)^2 = \left(\frac{154}{120}\right)^2$

This combination removes the ionosphere, troposphere, geometry and clocks contribution.

- Compute the Smoothed Code Differences (SCD) combination defined as follows

$$SCD_X(t) = M_{S_{X}^{+}{}_{m,n}}(t) - M_{S_{X}^{-}{}_{m,n}}(t-1),$$

where $M_{S_{X}^{+}{}_{m,n}}(t)$ denotes the *100* seconds smoothed, i.e. the averaged value, of code-carrier combination ($M_{C1_{m,n}}(t)$, $M_{P1_{m,n}}(t)$, or $M_{P2_{m,n}}$) over a sliding window containing the current sample plus the next *99* samples *[t, t+1,…, t+99]*, and $M_{S_{X}^{-}{}_{m,n}}(t-1)$ denotes the smoothed combination computed over a sliding window containing the previous *100* samples *[t-100, t-99,…, t-1]*.

Note: An independent SCD_X is computed for each code GPS (C1, P1 and P2).

- Compute the MEDIAN and MINIMUM values for each epoch having three or more stations detecting the anomaly simultaneously with the satellite in view.

- Anomalous behavior is declared at a given epoch *t* when the MEDIAN value is over a predefined threshold for a given code GPS (C1, P1 or P2).

Comment:

The same (code-minus-carrier) signal test $M_{PX_{m,n}}(t)$ could also be used to define a code pseudorange Jump, Drift and Acceleration monitor, by fitting a second order polynomial degree over a large time window (e.g. 100 seconds), in order to try to mitigate the multipath and code noise. Nevertheless, this approach will require to use large thresholds in order to reduce the chances of fault detections. On the other hand, drift and accelerations will be masked by code multipath.

Differential Code Bias jumps

The previous approach could be applied to monitor P2-P1 Differential Code Bias (DCBs) jumps, using as a signal test the next combination of code and carriers.

$$DCB_{P2-P1_{m,n}}(t) = R_{P2_{m,n}}(t) - R_{P1_{m,n}}(t) - \left(\Phi_{1_{m,n}}(t) - \Phi_{2_{m,n}}(t)\right),$$

Nevertheless, this monitor would be redundant with the previous one, as $DCB_{P2-P1_{m,n}}(t) = M_{P2_{m,n}}(t) - M_{P1_{m,n}}(t)$. Then, any event triggering this monitor, must be detected by the previous one.

DATA SET

The data set used in this study are 11 years of dual-frequency GPS measurement files at 1Hz, collected by a worldwide receivers network, gathered from the public domain server ftp://cddis.gsfc.nasa.gov/pub/gps/data/highrate in RNEX-2 file format [5].

Receivers type Selection

The following conditions have been applied to select the network of receivers, in order to assure enough satellite observability and reduce measurement noise:

- The satellite must be seen by at least three stations at any time.
- The elevation mask is 15º for carrier measurements and 20º for code measurements.
- The receiver's type should be as much homogeneous as possible (i.e. with similar figures of code and carrier noise) and the GPS receivers shall provide the C1, P1 and P2 codes.

The need of using a homogeneous set of receivers (i.e. with similar code noise) reduces the number of useful candidate sites. On the other hand, three stations with the satellite in common view is the minimum requirement in order to have a minimum redundancy for the monitors. However, in many cases, it is not enough to have a reliable anomaly detection, mainly for the code monitor, due to the code multipath.

Unfortunately, with the distribution of receivers available for this study, it has not been possible to guarantee the monitoring of the satellites the 100% of time when the previous conditions are meet. As an example, *Figure 1*, left hand plot, shows for a given week of 2014 (Days-Of-Year (DOYs) 067-073), the theoretical number of epochs with satellites in common view, as a function of the number of stations in the network and the elevation mask (considering the best possible homogeneous distribution). Fault-free receivers with 300 seconds sampling rate have been assumed to generate this plot. The curve in brown (ONLY ASHTEC: 40 STAS; ELEV>20º) corresponds to the selected network. Unfortunately, the number of ASHTEC receivers was decreasing at the end of the selected period (see *Figure 1*, right hand plot), being complemented with the JAVAD receivers available from 2012, which have a quite similar measurements quality. On the other hand, the selection is limited by the areas with a poor reference stations coverage (e.g. the oceans).

It is worth to say that co-located stations should be avoided. For instance, the carrier monitor can be triggered by scintillation and this could lead to detection events in case of having few stations available, e.g. in case of having only three stations and two of them co-located and experiencing scintillation.

Orbit and clock products

Precise orbit and clock products from IGS (final combined product) at 15 minutes and 5 minutes, respectively, have been used.

In the approach applied in this study, the monitoring of carriers is subjected to the availability of the IGS orbit and clock products, as they are used to remove geometry and satellite clock. This requirement can constitute a limitation "de facto", because the lack of these products is often linked to a satellite related problem.

Data pre-processing

The code and carrier measurements of the RINEX files available have been pre-processed to generate the input for the different monitors described in previous section. This pre-processing, basically consists in detecting cycle-slips and removing the geometry and satellite clocks, using the precise products. This data pre-processing can lead to the loss of some measurements due to the re-initialization of the cycle-slip detectors and monitors (10 and 200 seconds for carrier and code monitors, respectively) or to the availability of precise orbits and clock products.

The carrier monitor requires satellite orbits and clocks, thus this monitor is disabled when:

- IGS clocks are not available.
- IGS orbits cannot be interpolated. A maximum data gap of +/-1h around the interpolation epoch is established. It is worth to say that big data holes can produce large interpolation errors affecting the monitor performance, producing anomalous drift and accelerations.

The previous requirements are not needed by the code monitor, as it removes the geometry and clocks from a combination of carriers, i.e. neither orbit nor clock products are needed.

The cycle-slip detector used in this study implements evolutions of the algorithms defined in [8]. Moreover, it incorporates a conservative option that takes into account the Loss-of Lock-Indicator (LLI) given in the RINEX files, see [7] for more details. When this option is enabled, the detector declares cycle-slip any time that the LLI flag is set in the files.

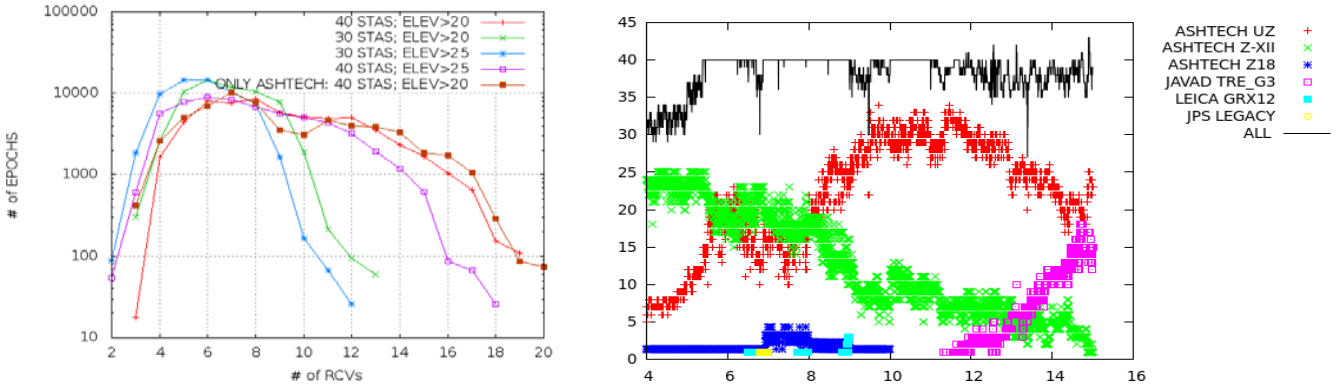

Figure 1. Left hand plot shows the theoretical number of epochs with satellites in common view by a given number of receivers along a week of 2104 (DOYs 067 to 073). Vertical axis is for the number of epochs and horizontal axis is for the number of receivers having satellites in common view. The different curves correspond to networks with different number of actual IGS stations at 1Hz and different elevation masks. Right hand plot shows the number of receivers available for this study. The horizontal axis indicates the year (from 2004 to 2016). The receiver type is indicated by different color. In black the total number of receivers available.

Finally, the satellite healthy status from RINEX navigation files (compiled by IGS) is always checked in order to account for the satellite condition.

DATA PROCESSING RESULTS

Monitor results characterization: Detection thresholds and values distribution

The selection of the anomaly detection thresholds would deserve a further discussion. In this study it has been applied an approach for experimental purposes. However, the thresholds may be set from an operational point of view considering the associated application or service and the level of tolerable error by the user.

Obviously, it can be run the monitors without setting detection thresholds, but when processing a huge amount of data as in this case (11 years at one-second sampling rate), the storage and CPU requirements for saving the results become very demanding and the processing time can last for several months. Fixing predefined thresholds, and saving only the data for further analysis when detecting anomalies allows to significantly reducing the storage and data handling requirements.

In this work, we initially used conservative thresholds (i.e. small thresholds), at expenses of increasing fault detections. Such small thresholds allowed us to revisit the results using other larger thresholds, in order to limit the number of events to analyze, because the data was already stored for a further analysis when the monitors were over the thresholds.

Table 1 and Table 2 show 99.99th percentile, maximum absolute deviation and the final selected thresholds for the carrier and code monitors over the 11-year period analyzed. Only epochs having the satellite in view from five or more stations have been considered to generate these tables in order to reduce the noise and to assure more redundancy in the results.

Table 1. Carrier monitor: 99.99th percentile, maximum values and thresholds, computed merging the absolute values of all satellites over the 11 years analyzed period.

Carrier	99.99%		Max		Threshold
	L1	L2	L1	L2	L1/L2
Jump (cm)	1.79	1.79	272.67	272.68	20
Drift (cm/s)	3.82	3.83	177.44	177.61	20
Accel. (cm/s^2)	0.20	0.20	24.16	24.14	2

Table 2. Code monitor: 99.99th percentile and maximum values and thresholds, computed merging the absolute values of all satellites over the 11 years analyzed period.

Code	99.99%			Max			Threshold
	C1	P1	P2	C1	P1	P2	C1/P1/P2
100s Step (m)	0.45	0.31	0.33	4.07	4.12	6.43	1.7

Detected events: Carrier monitor

In total, 124 days having carrier-phase events (on L1 and/or L2) have been identified over the 11 years period (January 1st 2004 to December 31st 2014), affecting 23 satellites. From these days, 72 are associated to the satellite SVN 063 from February 2012 to February 2014, which anomalous behavior was already reported in [9] when analyzing the GPS DCBs over the last 18 years. The SVN 063 behavior from 2012 to 2015 is illustrated in Figure 2. No multiple satellite events have been found in the same day. The list of events, excluding the 72 days of SVN 063 is given in Table 8, at the end of this paper.

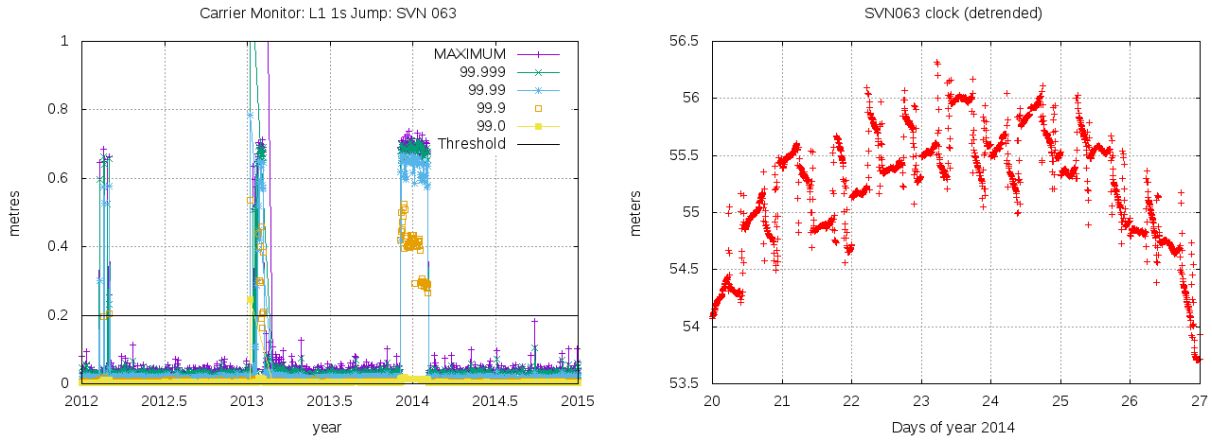

Figure 2. Left hand plot shows the percentiles and maximum value of carrier jump monitor for satellite SVN 063 from 2012 to 2015. Right hand plot shows and example of the anomalous behavior of satellite clock of SVN 063, depicted from the detrended precise clock, along a week on January of 2014.

After analyzing in detail such events, they have been classified in three different categories (see Table 8):

- Related with satellite clock oscillations: 13 days
- Related with satellite clock jumps: 32 days
- Related with satellite clock pulses: 4 days

There are some cases that can be seen as a mixture of clock oscillations and jumps: 3 days + (72 on SVN 063)

Example 1: Event related with a Satellite Clock Oscillation.

Table 3 summarizes the description of an event detected with the carrier monitors produced by a satellite clock oscillation. This event was experienced by satellite GPS SVN 046 on 8 March 2004 (Day of Year 068). The first detection is at 13:21:59 (48119 seconds of day) and last for 398 seconds, with 114 detections in this time interval (i.e. with Jump, Drift or Acceleration value over the threshold). The maximum deviations (in absolute value) of Jump, Drift and Acceleration found in this time interval are of 2.36 m, 1.27 m/s and 0.23 m/s2, respectively. The minimum deviations are 0.016 m, 0.001 m/s and 0.000 m/s2.

The detection of this event by the carrier monitors is depicted in the left hand plot of Figure 3. Similar detection patterns are found for the Jump and Acceleration monitors. The gap in the plot is due to the lack of measurements of at least three stations with the satellite in view in that time interval.

The analysis of this event is shown in the right hand plot of Figure 3, where the ionosphere-free combination of L1 and L2 carriers, corrected by the geometric range, satellite clock (from interpolated IGS product at 300 seconds) and receiver clock, along a continuous carrier phase arch, is shown for three different stations with the satellite in common view. As it can be seen, a common oscillation in the analysis period is experienced by the carrier measurements of these three stations, which are placed at different locations far away: MAS1, in Canary Islands, KOUR, in French Guyana, and VILL, close to Madrid in Spain.

Table 3. Description of carrier event experienced by SVN 046 on 8 March 2004 (Day of Year 068).

Signal	SVN	Date		Interval (sec)/Events			Maximum deviation			Minimum deviation			Thresholds		
		YY	DOY	Start Time	Time interv	Num. Events	Jump (m)	Drift (m/s)	Accel. (m/s2)	Jump (m)	Drift (m/s)	Accel. (m/s2)	Jump (m)	Drift (m/s)	Accel. (m/s2)
L1	046	04	068	48119	398	114	-2,364	1,272	-0,233	-0,016	-0,002	0,000	0,2	0,2	0,02
L2	046	04	068	48119	398	114	-2,362	1,271	-0,233	-0,016	-0,001	0,000	0,2	0,2	0,02

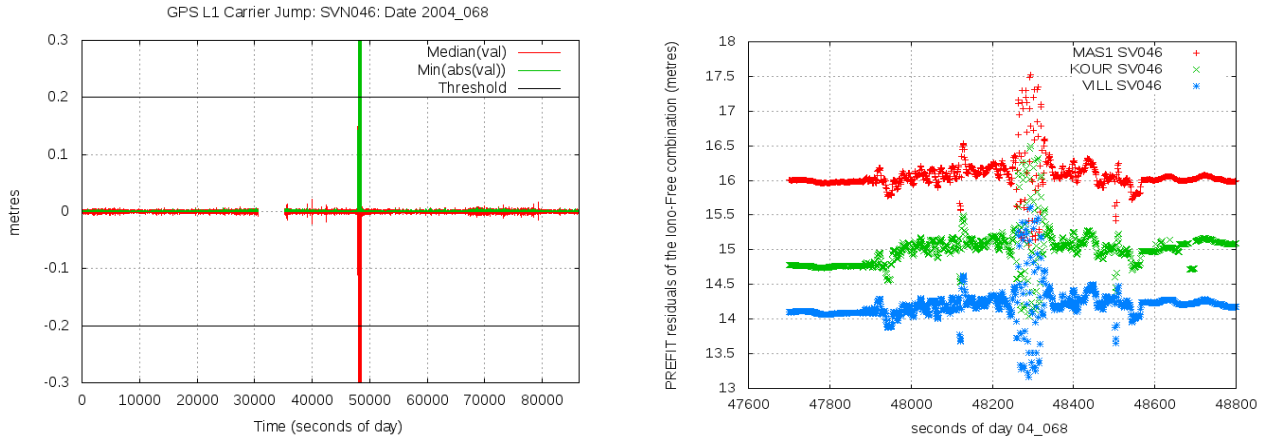

Figure 3. Analysis of SVN 046 event on 8 March 2004 (Day of Year 068). Left hand plot shows the event detection by the Carrier Jump monitor. Right hand plot shows the event analysis with the ionosphere-free combination of L1 and L2 carriers corrected by the geometric range, and satellite and receiver clocks (labeled as the PREFIT residuals). The pattern corresponds to the deviations of the actual clock from the linearly interpolated precise IGS clocks at 300 seconds. The same behavior is seen simultaneously by three different stations.

Example 2: Event related with a Satellite clock Jump.

In this second example, the carrier monitors detected an event at time 17:43:04 (63784 seconds of day) of the 23rd August 2004 (Day of Year 236), with 11 seconds of duration, see Table 4 and the left hand plot of Figure 4. This event performed as a sudden jump in the satellite clock, as depicted in the right hand plot of this Figure 4, where the evolution IGS clocks at 300 seconds is shown.

In order to have more insight about this anomaly, the left hand plot of Figure 5 shows the ionosphere-free combination of P1 and P2 codes, corrected by the geometric range and the receiver clock, but without correcting by the IGS interpolated clock. Notice from the right hand plot of Figure 4 that the clock drift of this satellite before and after the jump is less than 1mm /s, so that its effect in 300 seconds is less than one order of magnitude smaller than the clock jump. As it can be seen, the *code measurements* collected by the three different stations (MAS1, KOUR and VILL) experience a common jump at the time where the anomaly is detected by the monitor. On the other hand, we have also observed that this jump cancels in the geometry-free combination of codes (figure is not included to save space). Thence, taking into account that the previous depicted ionosphere-free combination of code measurements was only corrected by geometry and receiver clock (but not the satellite clock), this jump that can only be associated to a jump in the satellite clock.

Finally, it is interesting to note that a massive cycle-slip occurs in the carrier measurements collected by all stations with the satellite in view when this satellite clock jump happens. The effect of these cycle-slips are depicted in the right hand plot of Figure 5 by the jumps appearing in the geometry-free combination of carriers, in spite that this combination removes the clock.

Table 4. Description of carrier event experienced by SVN 030 on 23 August 2004 (Day of Year 236).

Signal	SVN	Date		Interval (sec)/Events			Maximum deviation			Minimum deviation			Thresholds		
		YY	DOY	Start Time	Time Interv	Num. Events	Jump (m)	Drift (m/s)	Accel. (m/s2)	Jump (m)	Drift (m/s)	Accel. (m/s2)	Jump (m)	Drift (m/s)	Accel. (m/s2)
L1	030	04	236	63784	11	11	2,074	1,418	-0,193	0,288	-0,015	0,001	0,2	0,2	0,02
L2	030	04	236	63784	11	11	2,076	1,417	-0,193	0,282	-0,014	0,001	0,2	0,2	0,02

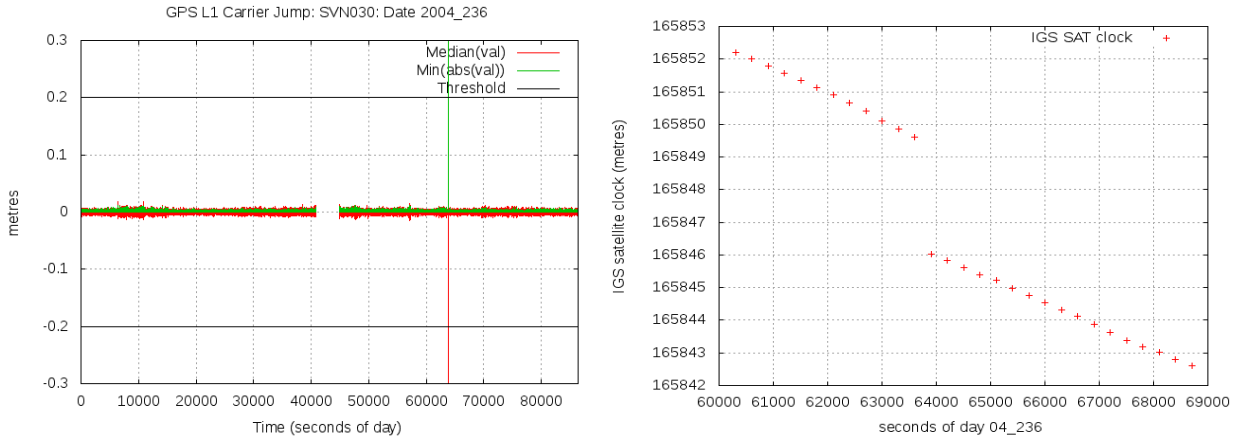

Figure 4. Analysis of SVN 030 event on 23 August 2004 (Day of Year 236). Left hand plot shows the event detection by the Carrier Jump monitor. Right hand plot shows the clock jump observed in the IGS precise clocks at 300 seconds.

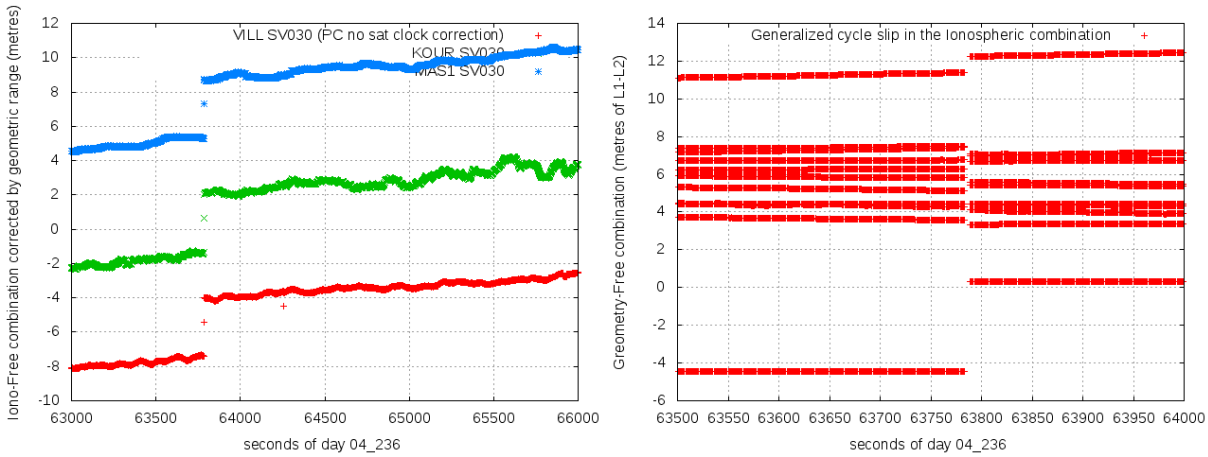

Figure 5. Analysis of SVN 030 event on 23 August 2004 (Day of Year 236). Left hand plot shows, for three different stations, the effect of the satellite clock jump in the ionosphere-free combination of P1 and P2 codes, corrected by the geometric range and receiver clock, but without correcting by the IGS interpolated clock. The right hand plot shows a massive cycle-slip experienced by all stations in the geometry-free combination of L1 and L2 carriers (cancelling the clock and geometry). This cycle-slip occurs when the jump in the satellite clock happens.

Example 3: Event related with a <u>Satellite Clock Pulse</u>.

A short duration event (9 seconds) is detected by the carrier monitors, affecting the satellite SVN 031 at time 00:35:52 (2152 seconds of day) of 16 November 2004 (Day of Year 321), see Table 5 and Figure 6, left hand plot.

A similar analysis as in the previous Example 1, using the ionosphere-free combination of L1 and L2 carriers corrected by the geometric range and satellite and receiver clocks, along a continuous carrier phase arch, is shown in the right hand plot of Figure 6. In this plot, a pulse of few seconds of duration is depicted from carrier measurements collected by two independent stations.

Table 5. Description of carrier event experienced by SVN 031 on 16 November 2004 (Day of Year 321).

Signal	SVN	Date		Interval (sec)/Events			Maximum deviation			Minimum deviation			Thresholds		
		YY	DOY	Start Time	Time Interv	Num. Events	Jump (m)	Drift (m/s)	Accel. (m/s2)	Jump (m)	Drift (m/s)	Accel. (m/s2)	Jump (m)	Drift (m/s)	Accel. (m/s2)
L1	031	04	321	2152	9	9	-0,282	0,242	-0,040	0,032	0,017	-0,006	0,2	0,2	0,02
L2	031	04	321	2152	9	9	-0,280	0,242	-0,040	0,030	0,017	-0,006	0,2	0,2	0,02

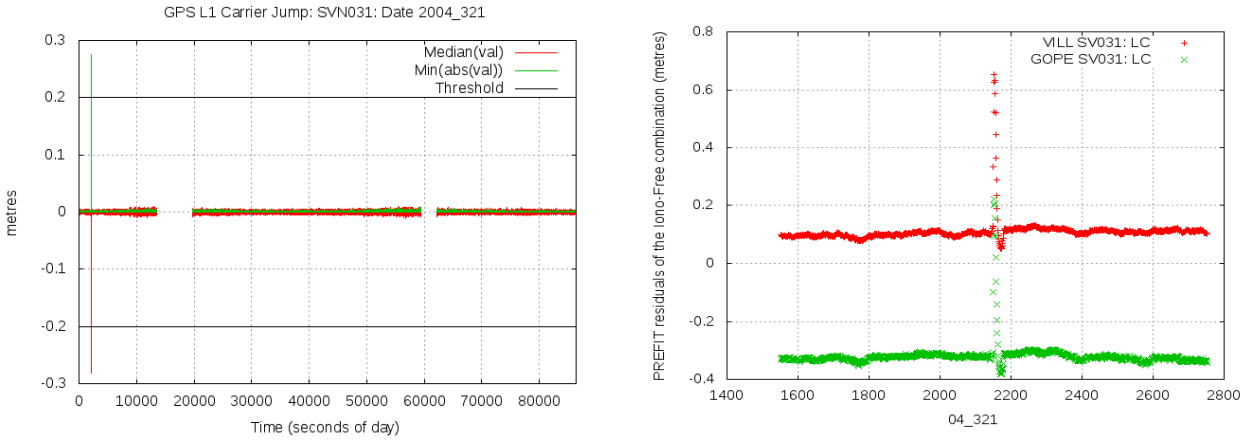

Figure 6. Analysis of SVN 031 event on 16 November 2004 (Day of Year 321). Left hand plot shows the event detection by the Carrier Jump monitor. Right hand plot shows the ionosphere-free combination of L1 and L2 carriers corrected by geometric range and satellite and receiver clocks. A short pulse of few seconds of duration is experienced simultaneously by the measurements collected from two different stations, VILL and GOPE.

Comments on carrier monitor detectability analysis

The carrier monitors are targeting to detect deviations from a linear/quadratic trend between satellite clock precise determinations every 300 seconds, in order to identify short duration events that could affect the user performance. In this way, long term trends are not considered a threat here, provided that they can be tracked by the reference stations and removed by linearly/quadratic extrapolation of differential corrections at a given sampling rate (in our case we use 300 seconds).

Thence, the next points must be taken into account when assessing the detectability for carrier monitor:

1. The carrier Jump, Drift and Acceleration detectors implemented in this work are monitoring only clock deviations from the linearly interpolated IGS precise clocks (provided every 300 seconds).
2. This means that, in particular, these monitors are not sensitive to the accumulated effect of drifts beyond 300 seconds.
3. They are able to detect one second jumps (because we use carriers at one second sampling rate) and drifts or accelerations (relative to the interpolated IGS clocks) over the predefined thresholds.

Figure 7 and Figure 8 illustrate an example of long-term satellite clock drift not affecting the carrier monitor. Indeed, the left hand plot of Figure 7 shows the behavior of carrier drift monitor for satellite SVN 033 on 31 July 2006 (Day of Year 212), which is far from the threshold although, as shown in the right-hand plot of Figure 7, there was a sudden change of clock drift within the monitored time interval (around 77000 seconds).

The explanation of such un-detectability is depicted in Figure 8, left hand plot, where it is shown the ionosphere-free combination of carriers after removing the geometric range, the lineally interpolated satellite clock from 300 seconds samples, and the receiver clock for two different stations with the satellite SVN033 in view: the stations QUIN (red) and AMC2 (green). The same values, but without removing the interpolated precise IGS clocks are shown in the right hand plot of Figure 8.

As the IGS clocks are updated every 300 seconds, they absorb the change in the satellite clock drift (see Figure 8, right hand plot). Thus, only the residual drift “relative to the IGS clocks” is seen by our monitors.

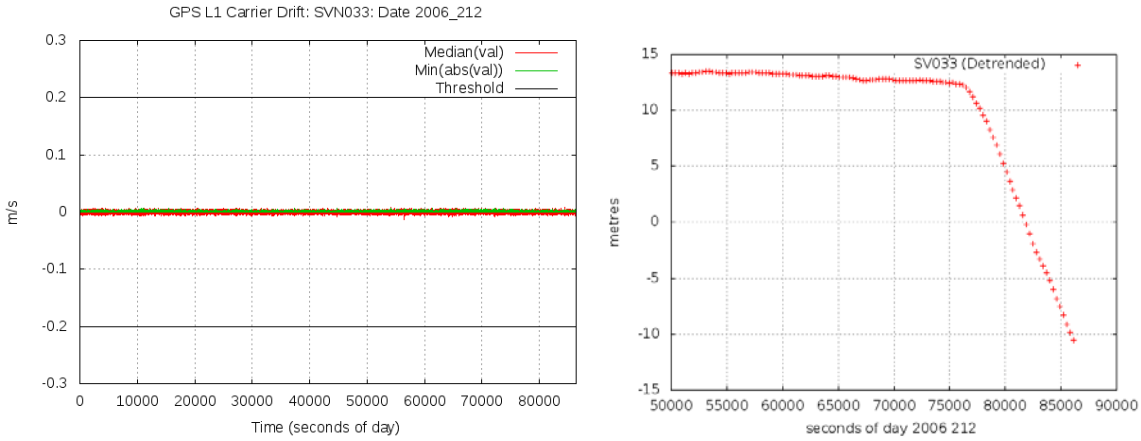

Figure 7. Analysis of SVN 033 drift on 31 July 2006 (Day of Year 212). Left hand plot shows the carrier Drift monitor behavior, which is far from detecting any event. The right hand plot shows the satellite clock estimated by IGS, detrended to depict the change in the slope (i.e. the drift).

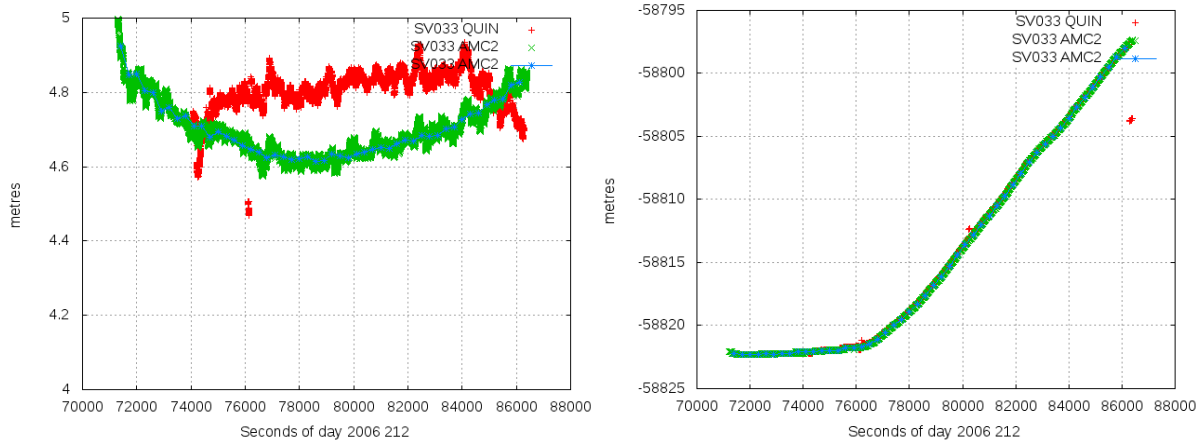

Figure 8: Analysis of SVN 033 drift on 31 July 2006 (Day of Year 212). Left hand plot shows the ionosphere-free combination of L1 and L2 carriers of stations QUIN (red) and AMC2 (green), after removing the geometry and the satellite clock, linearly interpolated, and the receiver clock. The blue line shows with stars, the values at the epochs in which the IGS clocks are given (i.e. every 300 seconds) for station AMC2. The right hand plot shows the same values, but without removing the interpolated precise IGS clocks.

Detected events: Code monitor

Except in one case, all events found by the code monitor are due to multipath. Indeed, in most of the cases there were only three stations with the satellite in view in the selected network, being the MEDIAN value used as the statistic to identify the events dominated by multipath. This also occurred in many other cases having 4 and even 5 stations with the satellite in view.

Code event: Jump on P1 code
A code event has been detected affecting the GPS SVN 061 on 3rd November 2013 (Day of Year 307) at time 08:53:33 (32113 seconds of day), see Table 6 and Figure 9, left hand plot.

A shown in Figure 9, right hand plot, this event is produced by successive jumps in the P1 code. These jumps trigger several detections of Code-Carrier-Incoherency monitor along the day. There is a gap between 36000 and 58000 seconds of day, produced by the lack of measurements from stations having the satellite in common view.

Table 6. Description of code event experienced by SVN 061 on 3 November 2013 (Day of Year 307).

CCI 100s Step	SVN	Date		Interval (sec)/Events			Deviation		
		YY	DOY	Start Time	Time Interv.	Num. Events	Max (m)	Min (m)	Threshold (m)
P1	061	13	307	32013	32606	375	2,895	1,701	1,7

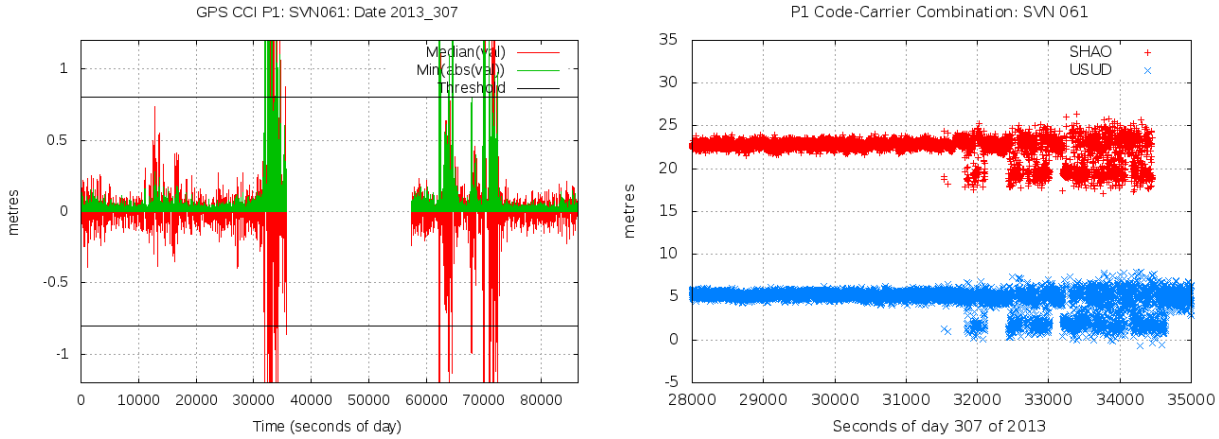

Figure 9. Analysis of GPS SVN 061 code event on 3 November 2013 (Day of Year 307). Left hand plot shows the P1 event detection by the Code-Carrier Incoherency monitor. Right hand plot depicts the P1 Code-Carrier Combination for SVN 061 computed from measurements collected by two different stations SHAO and USUD, experiencing the same trend of jumps.

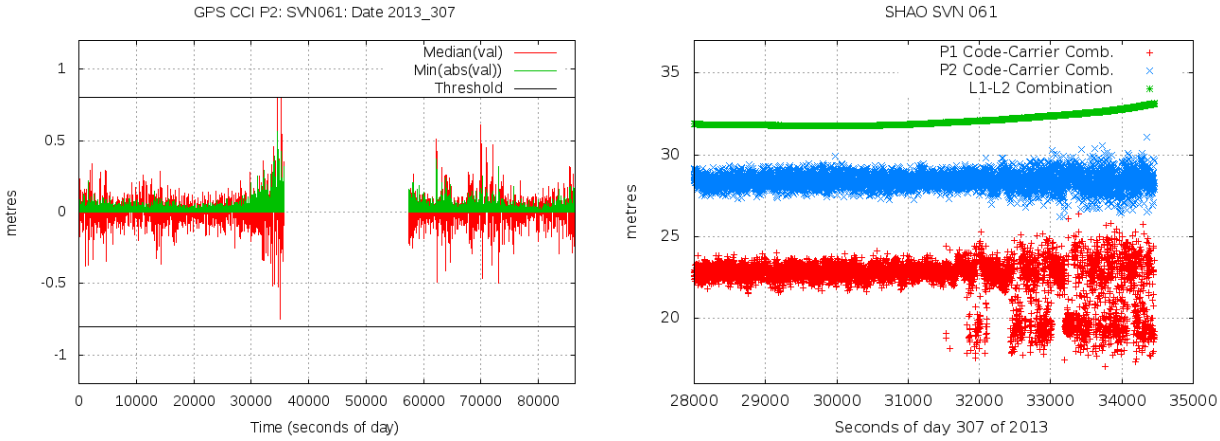

Figure 10. Analysis of GPS SVN 061 code event on 3 November 2013 (Day of Year 307). Left hand plot shows the performance of Code-Carrier Incoherency monitor on P2 code, which does not exceed the detection threshold. Right hand plot depicts for the SHAO station, the Code-Carrier Combination for P1 code, in red color, and P2 code, blue color. The geometry-free combination of L1 and L2 carriers is also shown in green to verify that no cycle-slip occurred during the jumps.

The monitor response to the P2 code is depicted in Figure 10, left hand plot. As shown, there is an increase of MEDIAN values after time 30000 seconds, but without exceeding the detection threshold. In this case, the enlargement is not linked to any SiS anomaly on P2 code, but to multipath, as confirmed by the right hand plot of Figure 10, where the Code-Carrier Combination is compared for P1 and P2 codes. The plot also includes the geometry-free combination of carriers in order to verify that no cycle-slip happened in the carriers, which could produce the jump of the P1 code.

CONCLUSIONS

A complementary detection methodology is presented in this paper, which is based on the use of code and carrier-phase measurements available from a set of IGS receivers worldwide distributed. The proposed methodology targets to detect code pseudoranges jumps and very short duration satellite clock events which most of them are undetectable through the processing of the precise IGS products. Over a period of 11 years of GPS L1 and L2 signals, more than $5x10^{10}$ values have been analyzed after running all monitors.

The data sets have been retrieved from public domain GNSS networks. A selection of a set of 40 stations worldwide homogeneously distributed (as much possible) and with similar code noise have been used in order to guarantee that the satellites are in view simultaneously for at least three stations most of the time.

The characterization of satellite clock anomalies has been targeting to detect very short duration events (up to one second). The detection of anomalous navigation data, by comparing broadcast ephemeris with IGS precise products, was out of the scope of this study. A monitor based on single frequency carriers corrected by the geometric range and interpolated satellite IGS clocks at 300 seconds sampling rate has been designed and applied to this study. This monitor is targeting to detect deviations from a linear/quadratic trend between satellite clock precise determinations every 300 seconds. Thence, long term trends are not considered a threat here, provided that they can be tracked by the reference stations and removed by linearly/quadratic extrapolation of differential corrections at a given sampling rate (in our case we use 300 seconds).

A total of 124 days having satellite clock events have been detected in the 11 years analyzed period, involving 23 different satellites and being 72 of them associated to SVN063. No multiple satellite events have been found in the same day. A detailed analysis of the detected events using this carrier based monitor (Carrier Jump, Drift and Acceleration) has shown that all of them are related with satellite clock anomalies in the GPS satellites. These anomalies can be classified in three different groups: clock oscillations, clock jumps and clock pulses, or combinations between them.

The code monitor based in the code-minus-carrier combination is targeting to detect code pseudorange jumps. This monitor uses single frequency code measurements corrected by the geometric range, satellite and receiver clocks and atmospheric propagation errors by a combination of two frequency carriers.

Only one event has been detected assessing the GPS codes. This event occurred on 3 November 2013 (Day of Year 307), and was experienced by GPS satellite SVN 061. It affected the P1 code, but not P2, neither C1. In all other cases, the detection was produced by code multipath, due to the few number of stations having the satellite in common view (three to five). Indeed, the statistic used to remove the outliers, i.e. the MEDIAN, was not able to filter out the effects of code noise.

REFERENCES

[1] Global Positioning System Standard Position Service Performance Standard, 4th Edition, September 2008.

[2] T. Walter and J. Blanch, “Characterization of GPS Clock and Ephemeris Errors to support ARAIM,” in Pacific PNT Meeting, Honolulu, HI, April 20-23.

[3] Heng, L. (2012). “Safe satellite navigation with multiple constellations: global monitoring of GPS and GLONASS signal-in-space anomalies”, Doctoral dissertation, Stanford University, 2012.

[4] Heng, L., Gao, G. X., Walter, T., and Enge, P. (2010). “GPS ephemeris error screening and results for 2006-2009”. In Institute of Navigation - International Technical Meeting 2010, ITM 2010 (Vol. 2, pp. 1184-1192).

[5] G. X. Gao, H. Tang, J. Blanch, et al., (2009). “Methodology and case studies of signal-in-space error calculation: top-down meets bottom-up,” Proc. ION GNSS, 2009.

[6] G. Xie Optimal on-airport monitoring of the Integrity of GPS-based Landing Systems. Doctoral Dissertation to the Electrical Engineering department of Stanford University, March 2004.

[7] RINEX version 2: ftp://igs.org/pub/data/format/rinex210.txt

[8] J. Sanz, JM. Juan, M. Hernández-Pajares. GNSS Data Processing. Volumes 1 and 2. ESA TM-23/1, May 2013, ISBN 978-92-9221-7.

[9] Sanz J., Juan, J.M., Rovira-Garcia A.,González-Casado G. (2017). "GPS differential code biases determination: methodology and analysis", GPS Solutions, October 2017, Volume 21, Issue 4, pp 1549–1561 DOI: 10.1007/s10291-017-0634-5.

Signal	SVN	Date		Interval (sec)/Events			Maximum deviation		
		YY	DOY	Start Time	Time Interv.	Num. Events	Jump (m)	Drift (m/s)	Accel. (m/s2)
L1	046	04	68	48119	398	114	-2,364	1,272	-0,233
L2	046	04	68	48119	398	114	-2,362	1,271	-0,233
L1	045	04	220	74762	130	37	-0,867	0,427	-0,073
L2	045	04	220	74762	130	37	-0,867	0,428	-0,073
L1	030	04	236	63784	11	11	2,074	1,418	-0,193
L2	030	04	236	63784	11	11	2,076	1,417	-0,193
L1	027	04	242	2402	52	11	0,213	0,222	0,036
L2	027	04	242	2402	52	11	0,213	0,222	0,036
L1	043	04	295	9661	637	93	-2,727	-1,378	-0,242
L2	043	04	295	9661	637	92	-2,727	-1,377	-0,241
L1	031	04	321	2152	9	9	-0,282	0,242	-0,040
L2	031	04	321	2152	9	9	-0,280	0,242	-0,040
L1	046	05	37	48391	400	107	1,304	-0,791	0,148
L2	046	05	37	48391	400	105	1,304	-0,790	0,148
L1	038	05	144	82302	1130	6	0,136	0,105	-0,028
L2	038	05	144	82302	1130	6	0,135	0,105	-0,028
L1	040	05	218	4510	2	2	0,255	0,125	-0,030
L2	040	05	218	4510	2	2	0,254	0,125	-0,030
L1	015	05	228	70002	9	4	-0,263	-0,141	-0,021
L2	015	05	228	70002	9	4	-0,264	-0,141	-0,022
L1	038	05	234	34114	2	2	-0,128	-0,088	0,023
L2	038	05	234	34114	2	2	-0,129	-0,088	0,023
L1	029	05	249	62464	11	11	2,191	1,495	-0,204
L2	029	05	249	62464	11	11	2,192	1,495	-0,204
L1	038	05	257	20953	171	5	-0,109	-0,075	0,023
L2	038	05	257	20953	171	5	-0,108	-0,076	0,023
L1	015	05	287	19840	11	8	0,578	-0,361	0,062
L2	015	05	287	19840	11	8	0,577	-0,361	0,062
L1	040	05	348	66484	11	11	2,065	1,414	-0,193
L2	040	05	348	66484	11	11	2,065	1,414	-0,193
L1	025	05	360	67983	97	28	-0,568	0,546	0,073
L2	025	05	360	67983	97	28	-0,567	0,546	0,073
L1	025	06	35	55296	8	6	-0,212	0,208	0,026
L2	025	06	35	55296	8	6	-0,214	0,209	0,026
L1	038	06	67	4342	16	16	0,979	0,781	-0,132
L2	038	06	67	4342	16	16	0,977	0,781	-0,132
L1	025	06	72	69244	11	11	2,066	1,354	-0,187
L2	025	06	72	69244	11	11	2,069	1,353	-0,187
L1	015	06	331	74584	11	11	2,190	1,437	-0,198
L2	015	06	331	74584	11	11	2,191	1,437	-0,198
L2	045	07	29	50407	1	1	-0,202	-0,001	0,006
L1	038	07	44	25383	3	3	0,149	0,135	-0,024
L2	038	07	44	25383	3	3	0,149	0,134	-0,024
L1	029	07	102	50935	4	4	0,092	0,076	-0,024
L2	029	07	102	50935	4	4	0,092	0,076	-0,024
L2	045	07	111	48167	1	1	0,230	0,057	-0,013
L1	035	07	118	86265	13	13	-0,555	0,502	-0,076
L2	035	07	118	86265	13	13	-0,555	0,503	-0,076
L1	037	07	229	7236	1	1	-0,092	-0,132	0,020
L2	037	07	229	7236	1	1	-0,092	-0,132	0,020

Signal	SVN	Date		Interval (sec)/Events			Maximum deviation		
		YY	DOY	Start Time	Time Interv.	Num. Events	Jump (m)	Drift (m/s)	Accel. (m/s2)
L1	040	07	262	27880	1990	8	-0,385	-1,058	0,127
L2	040	07	262	27880	1990	8	-0,402	-1,082	0,129
L1	030	07	341	54484	11	11	2,190	1,495	-0,204
L2	030	07	341	54484	11	11	2,190	1,494	-0,204
L1	058	08	93	5058	24497	22	-0,190	0,227	0,038
L2	058	08	93	5058	24497	22	-0,190	0,227	0,038
L1	024	08	178	63604	11	11	1,949	1,338	-0,183
L2	024	08	178	63604	11	11	1,950	1,338	-0,183
L1	023	08	209	11251	1	1	0,300	0,001	0,000
L2	023	08	209	11251	1	1	0,299	0,001	0,000
L2	045	08	360	45414	4	2	-0,243	0,142	-0,023
L1	030	09	166	61024	11	11	1,837	1,255	-0,172
L2	030	09	166	61024	11	11	1,837	1,256	-0,172
L1	038	09	296	28959	3	3	-0,172	-0,220	0,037
L2	038	09	296	28959	3	3	-0,171	-0,219	0,037
L1	034	09	310	78064	11	11	1,838	1,258	-0,172
L2	034	09	310	78064	11	11	1,837	1,258	-0,172
L1	035	11	208	56922	10	7	0,245	-0,226	-0,030
L2	035	11	208	56922	10	7	0,244	-0,224	-0,030
L1	023	11	325	80704	11	11	1,386	0,947	-0,129
L2	023	11	325	80704	11	11	1,385	0,947	-0,129
L1	033	11	355	67204	11	11	1,498	1,021	-0,140
L2	033	11	355	67204	11	11	1,500	1,020	-0,140
L1	035	12	23	24594	1	1	-0,058	-0,134	0,020
L2	035	12	23	24594	1	1	-0,058	-0,134	0,020
L1	026	12	39	67549	3469	3	-0,125	-0,126	0,023
L2	026	12	39	67549	3469	3	-0,125	-0,125	0,023
L1	026	12	43	8911	1	1	-0,090	-0,099	0,020
L2	026	12	43	8911	1	1	-0,091	-0,099	0,020
L1	036	12	103	49384	11	11	0,917	0,691	-0,093
L2	036	12	103	49384	11	11	0,919	0,690	-0,092
L1	027	12	265	52144	11	11	1,376	0,943	-0,129
L2	027	12	265	52144	11	11	1,375	0,943	-0,129
L1	054	13	49	75879	3	3	0,100	0,087	-0,024
L2	054	13	49	75879	3	3	0,099	0,088	-0,024
L2	034	13	63	63521	1	1	-0,209	-0,023	0,005
L1	026	13	100	60004	11	11	1,148	0,787	-0,108
L2	026	13	100	60004	11	11	1,151	0,787	-0,108
L1	035	13	114	59284	11	11	1,270	0,864	-0,118
L2	035	13	114	59284	11	11	1,271	0,864	-0,118
L1	023	13	175	44944	11	11	1,494	0,901	0,128
L2	023	13	175	44944	11	11	1,497	0,901	0,128
L1	033	13	203	72604	11	11	1,375	0,944	-0,129
L2	033	13	203	72604	11	11	1,376	0,943	-0,129
L1	062	13	230	51704	2389	8	0,375	0,155	0,022
L2	062	13	230	51704	2389	8	0,363	0,155	0,022
L1	036	13	255	61024	11	11	1,150	0,785	-0,107
L2	036	13	255	61024	11	11	1,150	0,784	-0,107
L1	035	14	281	41417	36791	769	0,446	1,774	-0,065
L2	035	14	281	41417	36791	768	0,447	1,776	-0,065

Table 8. L1 and L2 carrier detected events with the MEDIAN values of the Jump, Drift or Acceleration over the threshold. Maximum deviation of Median values in the time interval is in columns 8-10. The colors in the firsts two columns indicate: Yellow is for satellite clock oscillation events, brown is for satellite clock jump events and green for satellite clock pulse events. Mixed cases are indicated by two colors.